WILEY-VCH

Supporting Information

Realizing Highly Reversible $Nb^{5+}/Nb^{4+}/Nb^{3+}$ Redox Reactions in Bulk NASICON-$NaNbAl(PO_4)_3$ Anode Under Higher Current Rates

Ayon Phukan[‡, a], Biplab Patra[‡, a], Tanushree Acharya[b], Suraj Halder[c], Swathy Narayanan[a], Sheetal Kumar Jain[c], Gopalakrishnan Sai Gautam[b], Premkumar Senguttuvan* [a]

[a] New Chemistry Unit, International Centre for Materials Science, and
School of Advanced Materials,
Jawaharlal Nehru Centre for Advanced Scientific Research
Jakkur, Bangalore-560064, Karnataka, India.
E-mail: prem@jncasr.ac.in

[b] Materials Engineering
Indian Institute of Science
Bangalore-560012, Karnataka, India.

[c] Solid-state and Structural Chemistry Unit
Indian Institute of Science
Bangalore-560012, Karnataka, India.

[‡] These authors have contributed equally.

Experimental Details

Material Synthesis

NASICON-NaNbAl sample was synthesized by a conventional solid-state method. Na_2CO_3 (0.5 mmoles), Al_2O_3 (1.0 mmoles), Nb_2O_5 (1.0 mmoles) and $NH_4H_2PO_4$ (3 mmoles, 99%, Sigma) were used as the precursors for the synthesis of NASICON anode. Initially, all the precursors were well mixed using high-energy ball milling (SPEX 8000M) for 20 minutes. The ball-milled product was subsequently annealed at 400 °C for 5 hours. After annealing, the powdered material was shaped into a pellet of diameter 13 mm using a hydraulic press machine for homogeneous heating. The pellets were then sintered at various temperatures, including 850, 900, 950, and 1000 °C.

Material Characterization

The Rigaku Smart Lab diffractometer (Cu Kα; λ = 1.5406 Å) was used to measure XRD patterns of NASICON anodes at room temperature, with an accelerating voltage of 40 kV and a current of 30 mA. Rietveld refinements were performed on the collected XRD patterns using the FullProf Suite Program[1,2] to obtain structural solutions. The Zeiss (Gemini SEM 500) microscope was utilized to take field emission scanning electron microscopy (FE-SEM) images. Transmission electron microscopy (TEM; Thermofisher Talos F200 S) operated at 200 keV and equipped with a high-angle annular dark field (HAADF) detector and an energy dispersive X-ray spectrometer (EDS) was used to analyse morphology and distribution of elements. The Thermofisher K-Alpha instrument was used to perform X-ray photoelectron spectroscopy (XPS) measurements with micro-focused and monochromated Al Kα radiation with an energy of 1486.6 eV. The binding energy scale was calibrated from the C1s peak at 284.8 eV. The Avantage software was used to fit the core peaks with a nonlinear Smart-type background.

^{23}Na MAS Solid State NMR

^{23}Na solid-state magic angle spinning NMR (MAS NMR) has been conducted to obtain further information about the changes in local environments across the samples, and specifically the presence of mobile and relatively rigid Na atoms at their lattice points. A 500 MHz HRMAS solid-state spectrometer has been used to perform the 23Na NMR experiments at a MAS of 12.5 kHz (using a 4mm probe). The sample was packed inside an insert (volume of 25 µL), which was put inside the 4 mm rotor. For reference purposes, NaCl has been observed using the same parameters, and the same data is being used to analyse all the spectra quantitatively. For direct data collection, the length of the pulse was 3.5 µs, and the power level was 0 dB. To achieve a reasonable signal-to-noise ratio (SNR) for the deconvolution, we collected 4096 transients for each spectrum along with 30 ms of acquisition time, 1 s of recycle delay and 700 ppm of spectral width.

Electrochemical Measurements

To prepare the NASICON anodes, the active material and Super C45 (Timcal) were ball milled together in a weight ratio of 75:25 for 15 mins. Polyvinylidene fluoride (PVDF) binder was added to the ball-milled mixture, resulting in a final mass ratio of active material, C45 and PVDF of 70:22:8. In order to obtain the electrode slurry, an appropriate amount of N-methyl-2-pyrrolidone (NMP) solvent was added to the mixture and the slurry was uniformly coated on a carbon-coated Al foil followed by overnight drying in vacuum oven at 120 °C. The dried electrodes were calendared and punched into round disc electrodes with a 16 mm dia. cutter, and the active material of each disk was estimated as 3.0-3.5 mg cm^{-2}. For the electrochemical measurements, coin cells were used where sodium (99.9%, Sigma–Aldrich) metal acts as the counter electrode. 1M $NaPF_6$ in diglyme was used as the electrolyte for testing. The solvents were extensively dried on molecular sieves to capture the moisture. Whatmann Glassfibre (GF/D 150mm) filter papers of 19 mm diameter were used as separators.

The cells were assembled in an argon-filled glove box (MBraun; O2 < 0.1 ppm and H2O < 0.1 ppm) and galvanostatic charge/discharge tests were conducted using a battery cycler (BT-lab, Biologic) at different C-rates in the voltage window of 3.0–0.9 V versus Na^+/Na^0. Galvanostatic intermittent titration technique (GITT) experiment was performed after the third cycle. GITT measurements consisted of 0.5 h of charges or discharges at a C/10 rate, followed by a rest of 2 h to obtain a steady state.

In-situ XRD

In situ XRD measurements at C/10 rate were conducted using a Bruker D8 diffractometer (Cu-Kα source) with a custom-designed in situ cell featuring a beryllium (Be) window. A free-standing film of the NASICON anode was placed onto a pinhole-free thin aluminium foil (Alfa, 99.99%, 10 mm thickness) and strategically placed beneath the Be window. XRD patterns were collected at 30 min intervals at different states of charge while cycling the cell at a C/10 rate, within a voltage range of 3.0 to 0.9 V versus Na^+/Na^0. LeBail fittings were performed on the in-situ XRD patterns to determine cell parameters using the FullProf Suite Program. [1,2]

Operando XRD measurements at high rates (1C and 2C) were carried out at beamline P02.1[3,4] of PETRA III, DESY (Deutsches Elektronen-Synchrotron) in Hamburg, Germany, using synchrotron radiation with an energy of around 60 keV (λ = 0.20736 Å). The operando cells were custom-built in our laboratory in a coin-cell configuration with Kapton windows and assembled inside an argon-filled glovebox (H_2O and O_2 levels below 0.1 ppm). We used an eight-position coin-cell holder, connected to a BioLogic VMP-3 potentiostat and operated via EC-Lab software, as described previously.[5] Each cell was first pre-cycled at C/2 for one cycle to stabilize its performance before moving to high-rate cycling. The operando XRD data were collected across up to four cells simultaneously, with an acquisition time of one minute per cell before stepping to the next, resulting in a one-minute scan for each cell every six minutes. The diffraction patterns were analyzed using the FullProf App.[6]

XAS Measurements:

X-ray absorption spectroscopy (XAS) experiments were carried out at the P65 beamline of PETRA-III at DESY in Hamburg, focusing on both pristine and cycled electrodes at various states of charge. Spectra were obtained at the Nb K-edge utilizing a quick-XAS mode, which involved conducting three scans per sample, each lasting three minutes, in transmission mode. Gas ionization chambers were used to monitor the intensities of both the incident and transmitted X-rays. *Ex-situ* electrodes were collected at different charge states, sealed between Kapton tapes within an argon-filled glove box, and directly employed for data acquisition. All measurements were executed at room temperature, utilizing a Si (111) double-crystal monochromator, and the resulting data were analyzed using the DEMETER software package.[7,8]

Computational details:

All spin-polarised density functional theory (DFT) calculations for constructing the convex hull and voltage profile were performed utilizing the Vienna ab initio simulation package[9,10] and employing the strongly constrained and appropriately normed (SCAN)[11] functional for treating the electronic exchange and correlation. The core electrons were modelled using the frozen-core projector augmented wave[12] potentials. The plane wave basis was expanded up to a cutoff kinetic energy of 520 eV, and the convergence criteria for the calculations were set as 10^{-5} eV and |0.03| eV $Å^{-1}$ for the total energies and atomic forces, respectively. The irreducible Brillouin zone (IBZ) was sampled using a 4×4×4 Γ-centered *k*-point mesh (corresponding to a minimum mesh density of 32 *k*-points per Å). The lattice vectors, cell shapes, and cell volumes were relaxed without preserving any underlying symmetry. The electronic density of states (DoS) calculations for the ground state compositions were carried out with a minimum mesh density of 96 *k*-points per A to sample the IBZ and the convergence criterion for total energies was set to 10^{-6} eV.

We performed our DFT calculations on the primitive cell of the NASICON conventional cell (i.e., having a composition of $Na_8Nb_2Al_2(PO_4)_6$ or 2 formula units per cell) to reduce the computational costs. All possible symmetrically-distinct Nb/Al configurations at the as-synthesized $NaNbAl(PO_4)_3$ composition were enumerated using the pymatgen[13] package, while keeping all the Na(1) sites occupied by Na. This resulted in three unique Nb-Al configurations on which DFT calculations were done to identify the ground state Nb-Al configuration. Further, Na/vacancy orderings were enumerated, while keeping the Nb-Al ground state ordering of the as-synthesized composition, from x = 1 to 4 in $Na_xNbAl(PO_4)_3$ with a step size of $\Delta x = 0.5$, resulting in a total of 54 distinct configurations across all the compositions. We employed the MACE-MP0[14,15] model to pre-relax all the configurations, across the Na compositions. Subsequently, we performed DFT for the five lowest energy configurations, as determined by MACE-MP0, to determine the ground state configuration at each Na composition. Finally, we constructed the 0 K convex hull and calculated the Na-intercalation voltage profile, using methods described in previous studies. [16,17]

The migration barrier (E_m) for moving a Na atom sitting in the Na(1) site to an adjacent vacant Na(2) site was calculated using the nudged elastic band (NEB)[18] method in conjunction with DFT. For all DFT-NEB calculations, we used the generalized gradient approximation (GGA)[19] functional to model the electronic exchange and correlation instead of the SCAN

function, given that GGA provides qualitatively reliable trends in E_m at lower computational costs compared to SCAN[20]. For the NEB calculations, we used a lower mesh density of 16 *k*-points per Å to reduce computational expense. A total of seven intermediate images were used between the endpoints to model the minimum energy pathway (MEP), with a spring force constant of 5 eV $Å^{-2}$ maintained between adjacent images. The optimization of the images constituting the NEB was done using the limited-memory Broyden-Fletcher-Goldfarb-Shanno (L-BFGS)[21] method until the force component perpendicular to the elastic band fell below |0.05| eV/Å. We used the Orb-v3[22,23] model to obtain a better initial guess for the MEP before doing a DFT-NEB calculation, i.e., we used Orb-v3 as a pre-relaxation model for the NEB.[24]

Full Cell Fabrication:

The sodium ion full cells were fabricated using NVP as the cathode and NaNbAl as the anode. The synthesis of NVP was carried out, according to the literature. The NVP electrodes were prepared by mixing the active material, C45, and PVDF in a 70:22:8 weight ratio in the NMP solvent and the slurry was coated on carbon-coated Al-foil. The capacity ratio of anode/cathode is maintained as 1.06/1.0 in the full cell. The galvanostatic charge-discharge measurements of the full cells were carried out in the voltage window of 2.5-0.4 V at different C-rates. For the fabrication of full Na-ion cell, we precycled the NVP cathode within 3.8 V- 1.0 V for 3 cycles and collected the electrode at 1.0 V which provides $Na_4V_2(PO_4)_3$,[25] then clubbed with the NaNbAl anode. The energy density of Na_4VP||NaNbAl full sodium-ion cell was calculated by the following equation:

$$\boldsymbol{E = \frac{Q \times M_{cathode} \times V}{M_{cathode} + M_{anode}}}$$

Where E represents the energy density (Wh kg^{-1}), Q is the discharge capacity of the cell (mAh g^{-1}), V is the average voltage of the cell, $M_{cathode}$ and M_{anode} are the mass of the cathode and anode, respectively.

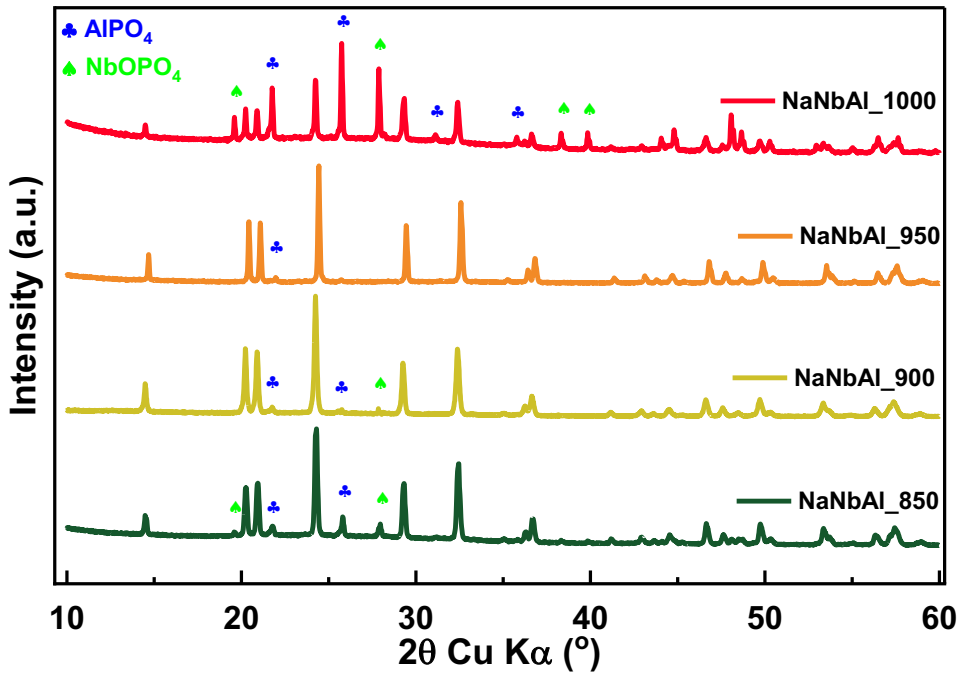

Figure S1. XRD Patterns of NaNbAl at different reaction temperatures (850, 900, 950, 1000).

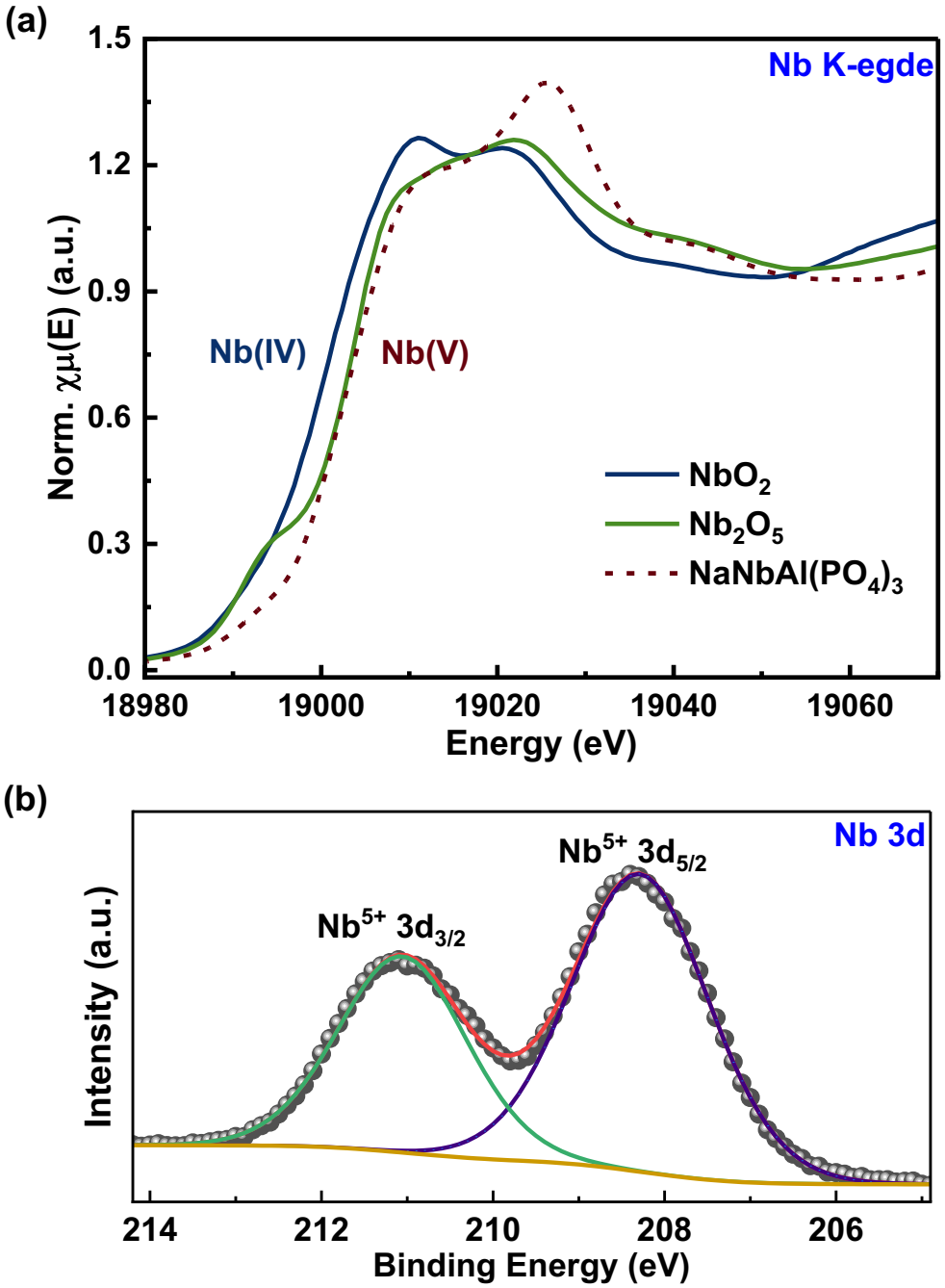

Figure S2. a) XANES spectra collected at the Nb K-edge and b) X-ray photoelectron spectroscopy (XPS) core level Nb 3d XPS spectra of the NaNbAl anode.

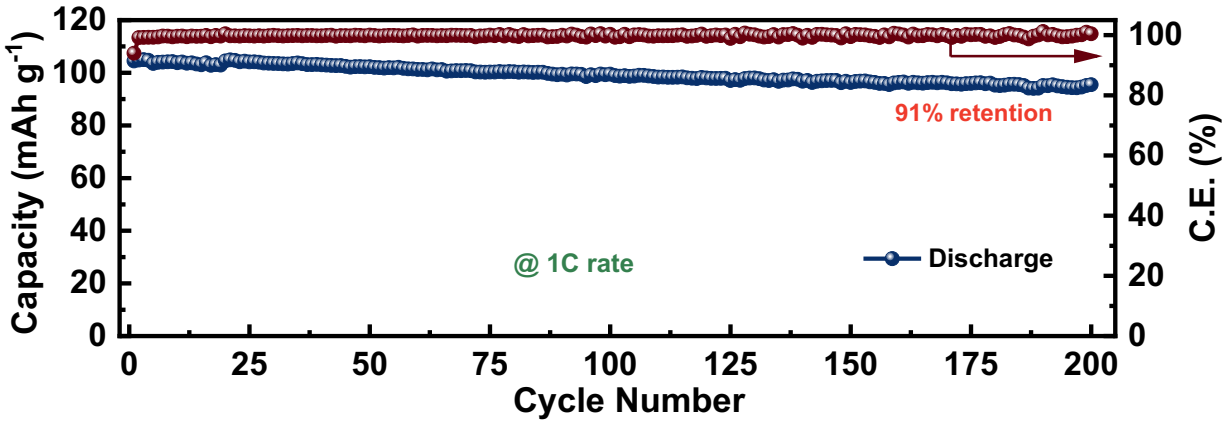

Figure S3. Long-term cycling stability of NaNbAl anode at 1C rate.

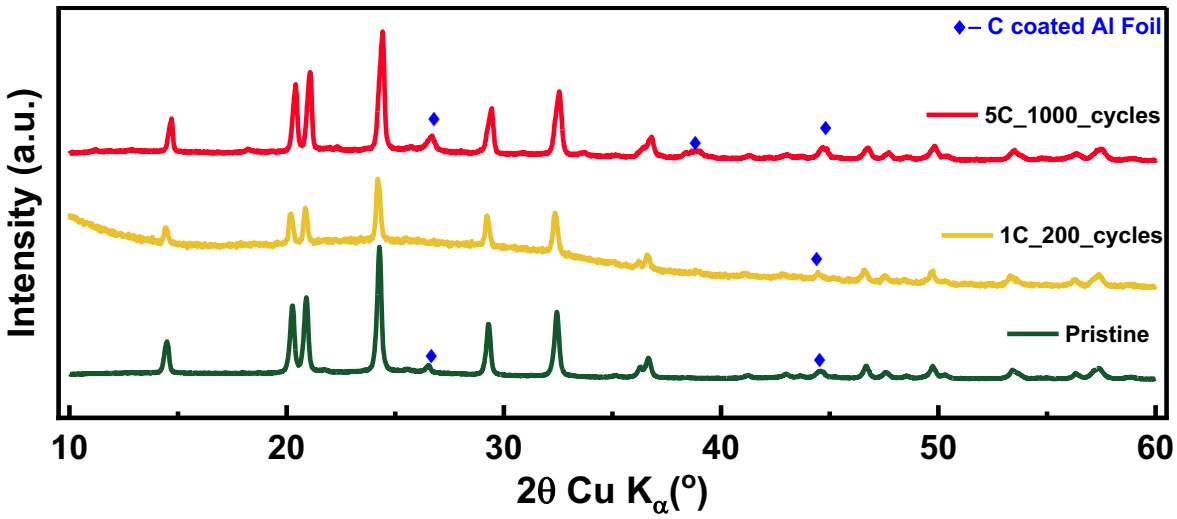

Figure S4. XRD patterns of pristine and cycled electrodes of NaNbAl anode.

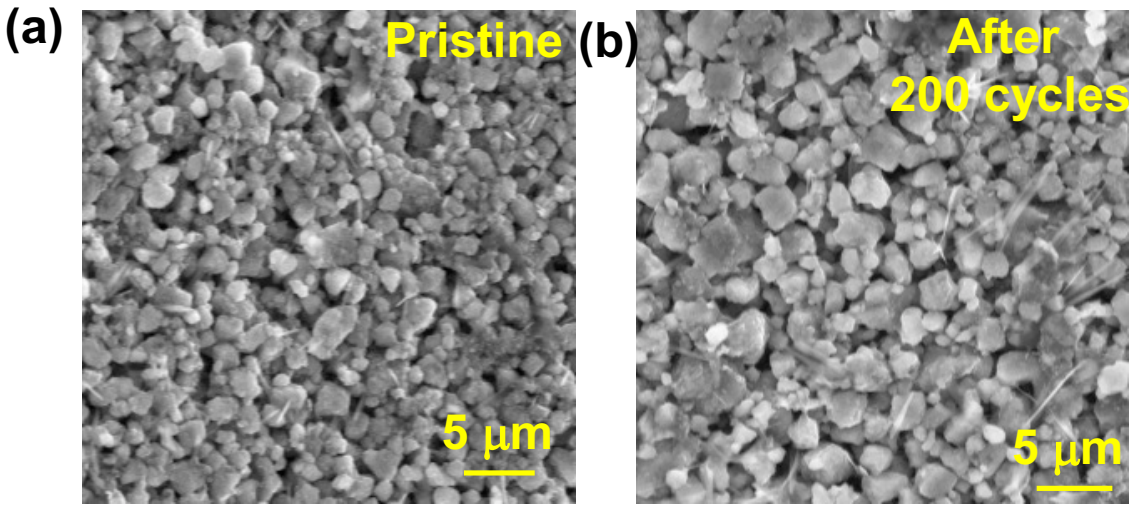

Figure S5. SEM images of (a) pristine electrodes and (b) after 200 cycles at 1C rate of NaNbAl anode.

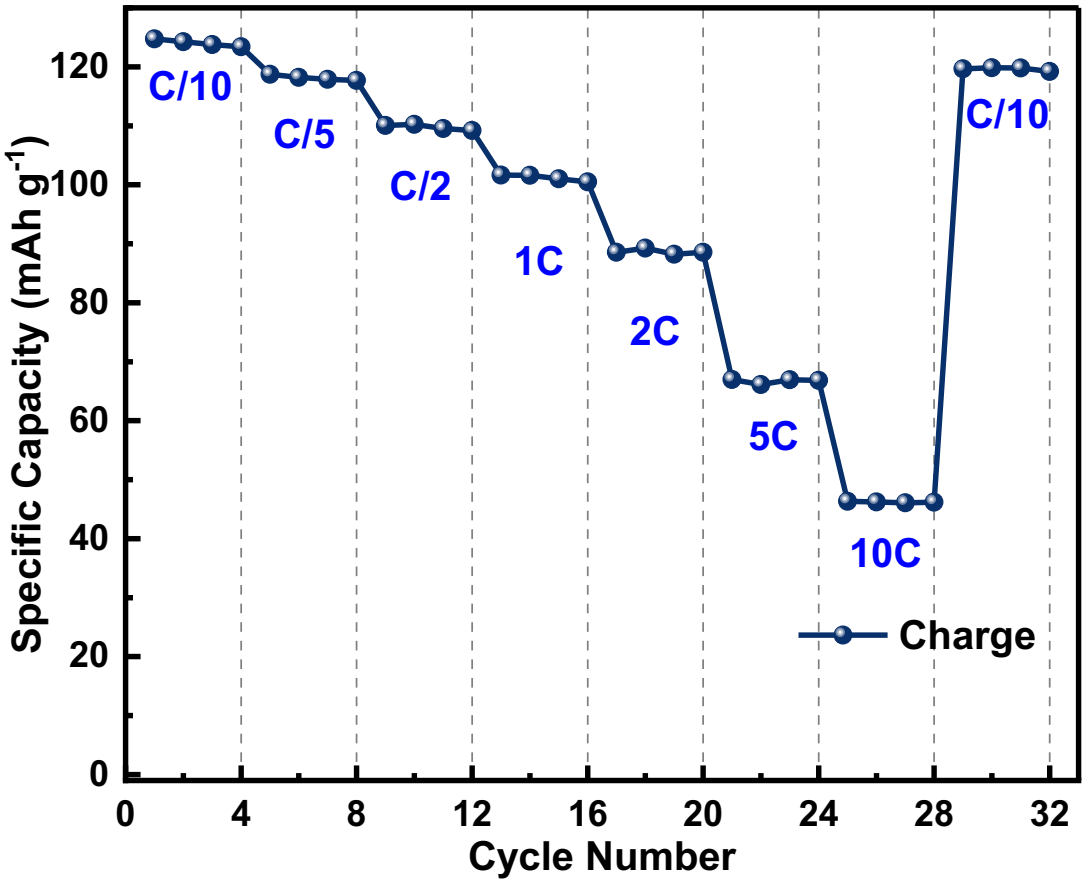

Figure S6. Rate Performances at various C rates C/10, C/5, C/2, 1C, 2C, 5C and 10C of the NaNbAl anode.

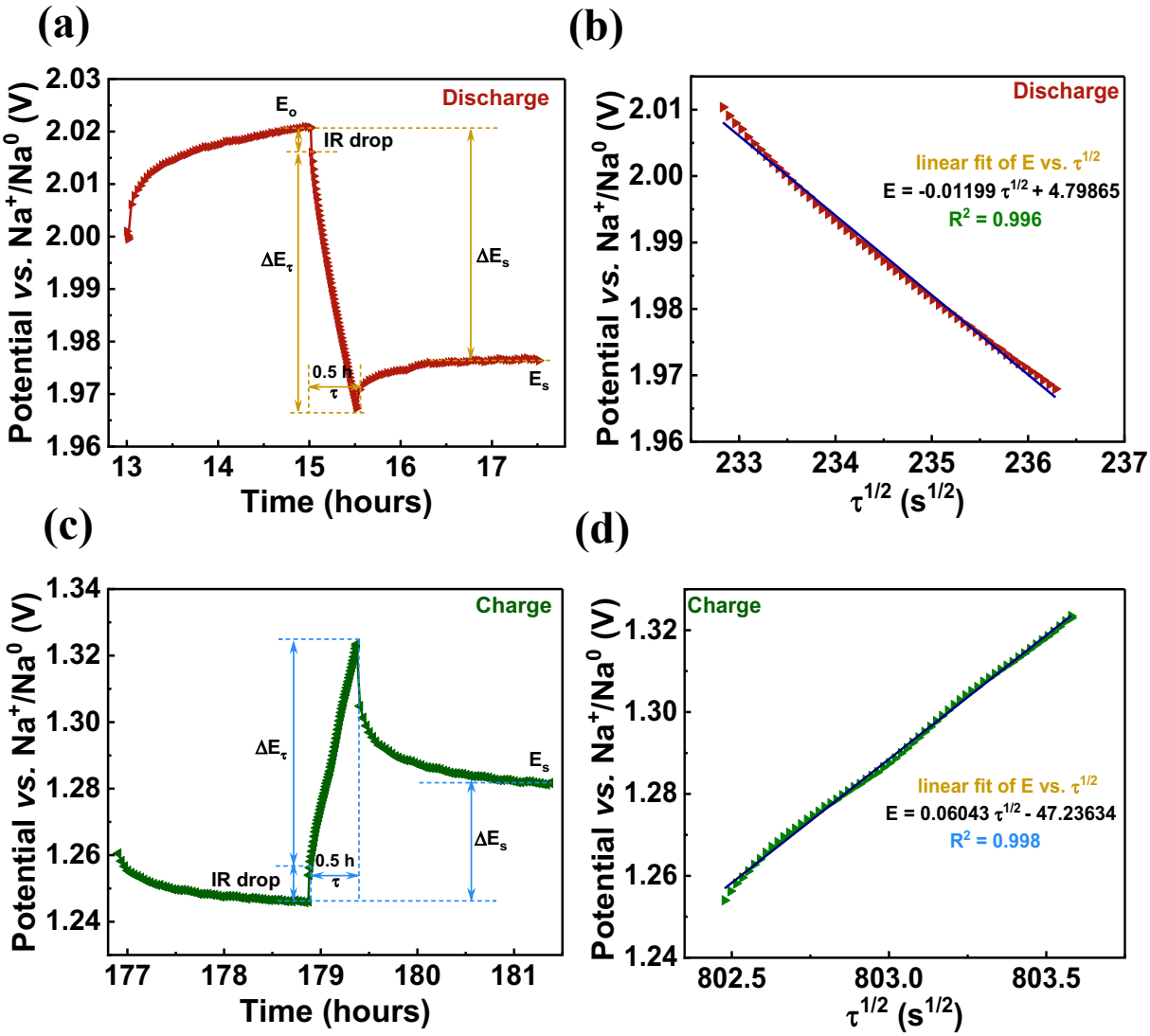

Figure S7. Potential vs. time curves of NaNbAl anode during (a) discharge and (b) charge processes at C/10 rate for a single step Galvanostatic intermittent titration technique (GITT).

Calculation of Diffusion Coefficient

The galvanostatic intermittent titration technique was utilised to investigate the Na-ion diffusion kinetics in the NaNbAl NASICON anode. During the GITT experiment, cells were cycled at a controlled C/10 rate for 30 minutes, followed by a 2-hour relaxation period to allow the voltage to stabilize and reach equilibrium. This process was repeated throughout the entire cycle to ensure thorough data collection. If the cell voltage variation during titration, plotted against $\tau^{1/2}$, demonstrates linear behaviour, the Weppner and Huggins equation[26] can be applied to calculate the diffusion coefficient (D_{Na+}), offering crucial insights into the ion transport dynamics within the anode. The equation is as follows:

$$D_{Na^+} = \frac{4}{\pi\tau}\left(\frac{m_B V_M}{M_B A}\right)^2 \left(\frac{\Delta E_s}{\Delta E_\tau}\right)^2 \qquad \left(\tau \ll \frac{L^2}{D_{Na^+}}\right)$$

where, τ = constant current pulse time (1800 s), m_B = active material mass(g), MB = molecular weight (g mol^{-1}), VM = molar volume (cm^3 mol^{-1}), A = total contacting area of electrode with electrolyte (cm^2). ΔE_s = voltage difference during the open circuit period, ΔE_τ = cell voltage change during a constant current pulse excluding the resistance (IR) drop, and L = average radius of the active material particles.

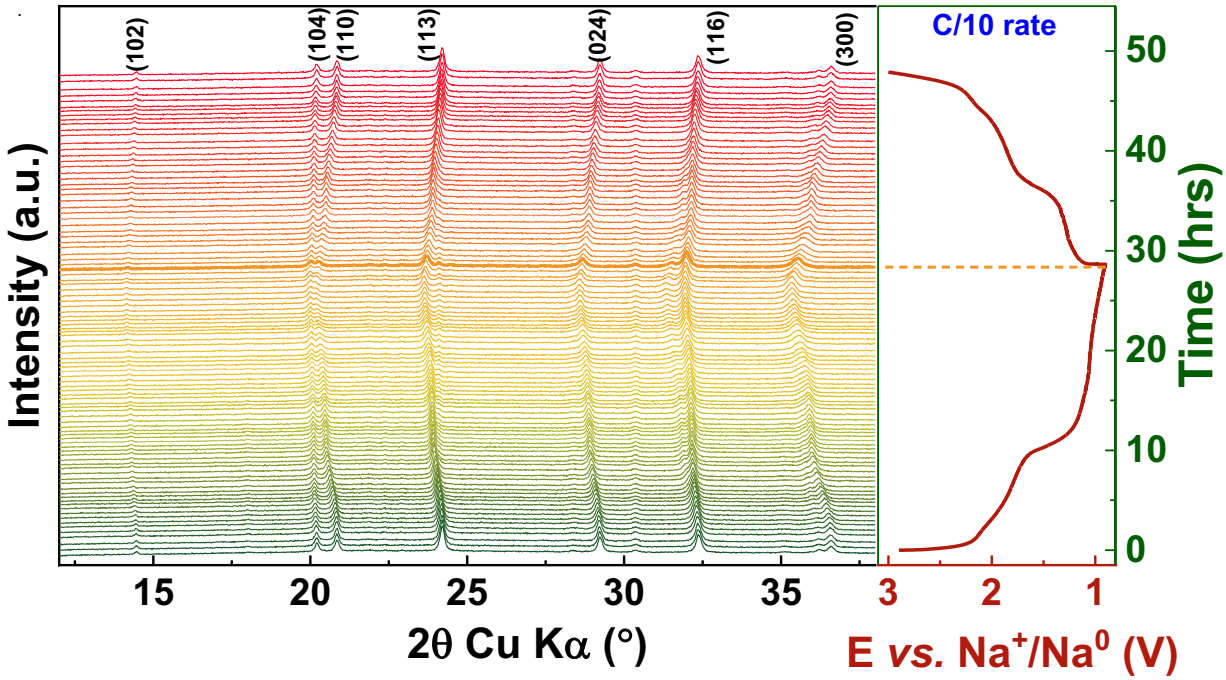

Figure S8. *Operando* XRD patterns of the NaNbAl anode collected at C/10 rate (lab scale).

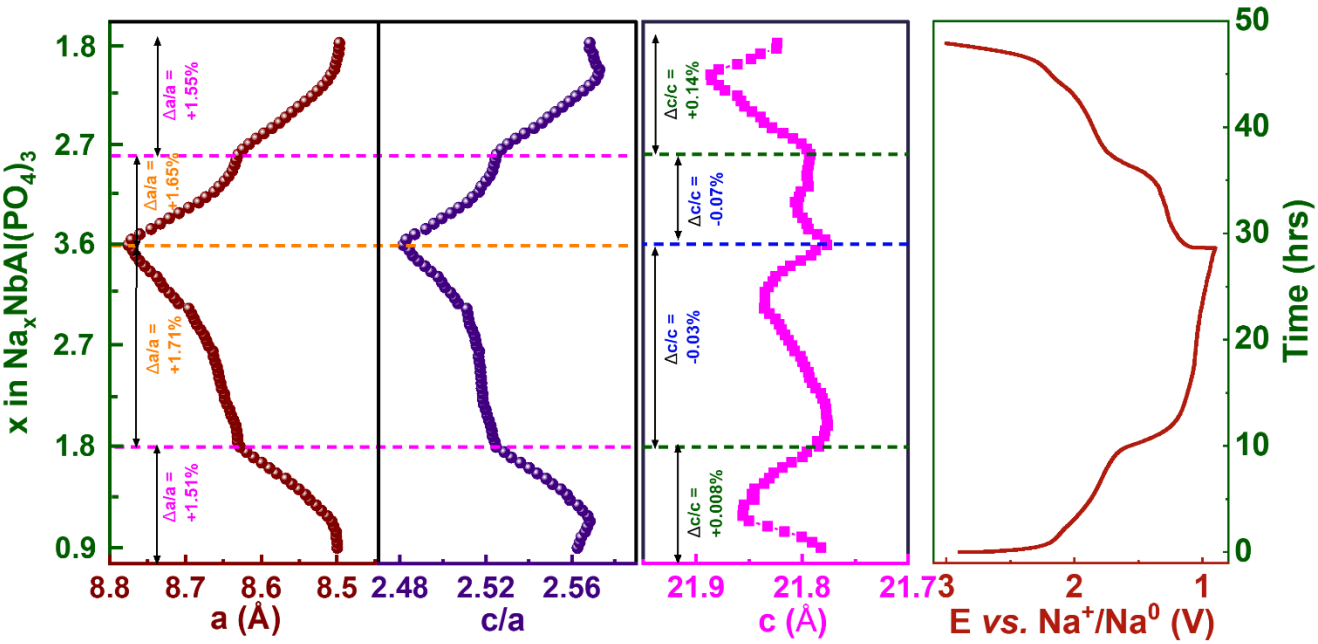

Figure S9**.** Lattice parameter evolution determined from *in-situ* XRD for NaNbAl anode during cycling at C/10 rate.

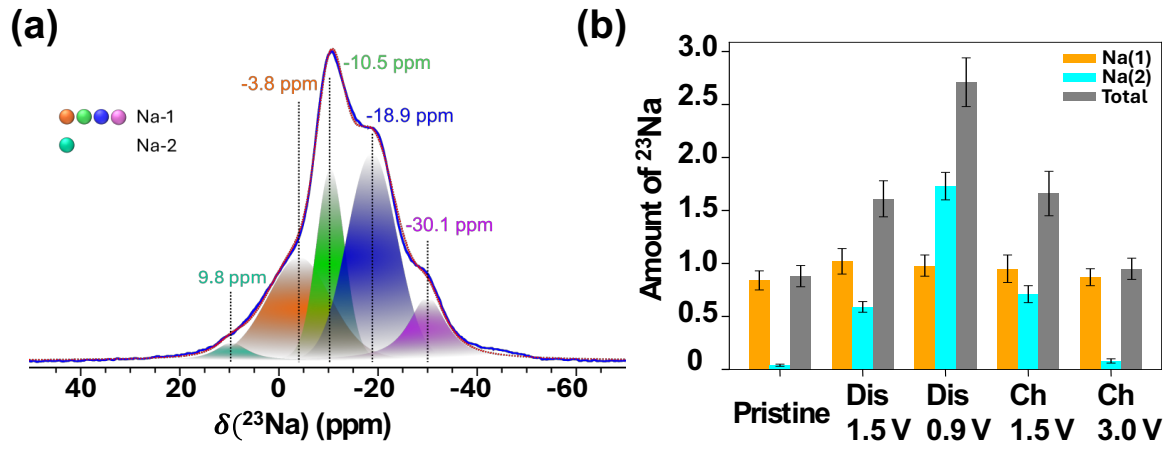

Figure S10. a) 12.5 kHz MAS NMR spectra of 23Na at Room temperature and assigning the peaks for Na(1) and Na(2) sites of Na present in the pristine sample. b) Quantitative analysis of Na(1) and Na(2) sites calculated from ex-situ NMR of Na throughout the cycle.

Peak Analysis of ^{23}Na NMR Spectra

We identified four distinct types of ^{23}Na peaks corresponding to the Na(1) site at -30.1 ppm, -18.9 ppm, -10.5 ppm, and -3.8 ppm, alongside a prominent peak at 9.8 ppm for the Na(2) site. The distribution of these Na site peaks exhibits subtle variations throughout the charge-discharge cycle, a change that is clearly depicted in the deconvoluted data presented in Fig. S10a. In our analysis, we also detected a remarkably small amount of Na(2) in the pristine sample, measuring 0.04±0.01 (equivalent to 4.76%±1.25%), which we highlighted in cyan in the NMR spectra. This fraction experiences a significant increase during the complete discharge of the sample, suggesting an infusion of sodium into the Na(2) sites, which subsequently decreases once the sample is fully charged again. This cycle indicates a dynamic process of filling the Na(2) sites, and the quantification of these changes is further illustrated in the accompanying bar diagram found in Fig. 10b.

Calculations of quantitative analysis

Deconvoluted peaks filled with different colours in each spectrum correspond to the ^{23}Na resonances that provide the fit of the experimental signal using the 'GAUSS+LORENTZ' fitting model, such that the line-width is a combination of Lorentzian and Gaussian contributions. The area under the peaks after deconvolution was used to calculate Na(1) and Na(2) sites quantitatively. The areas of each peak are taken using the SOLA package of Bruker 4.3.0 version. Different isotopic peaks of ^{23}Na, as shown in Figure 10b, colour-coded & deconvoluted. NaCl sample was used as reference for quantitative analysis. The amount of ^{23}Na can be calculated using the following formula,

$$\frac{Total\ area\ under\ the\ spectrum\ of\ the\ sample\ or\ a\ peak}{Total\ area\ under\ NaCl\ spectrum\ (with\ same\ parameters)} = \frac{Amount\ of\ Na\ in\ sample\ or\ interested\ peak}{Amount\ of\ 23Na\ in\ the\ NaCl}$$

This has been used to see the fractional or percentage calculations also.

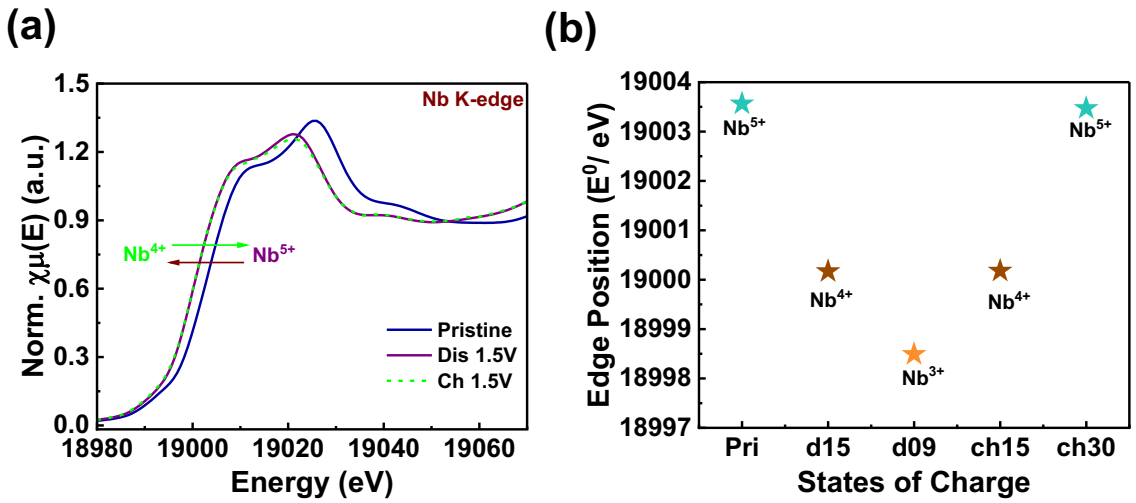

Figure S11. a) *Ex-situ* XANES plots (Pristine, Discharge 1.5V and Charge 1.5V) of the NASICON-NaNbAl anode collected at the Nb K-edge. b) Evolution of the edge positions of Nb K-edge of NaNbAl anode at different states of charge.

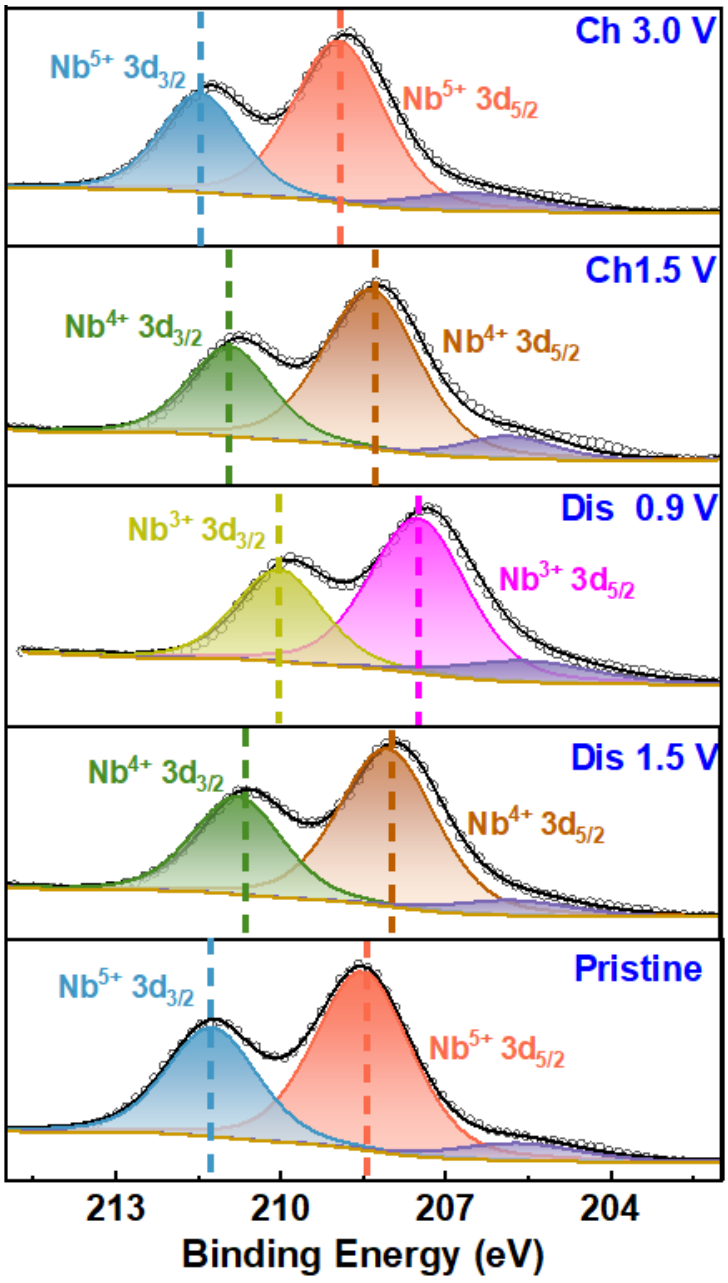

Figure S12. *Ex-situ* XPS of high-resolution Nb3d spectra of NaNbAl anode collected at different states of charge.

.

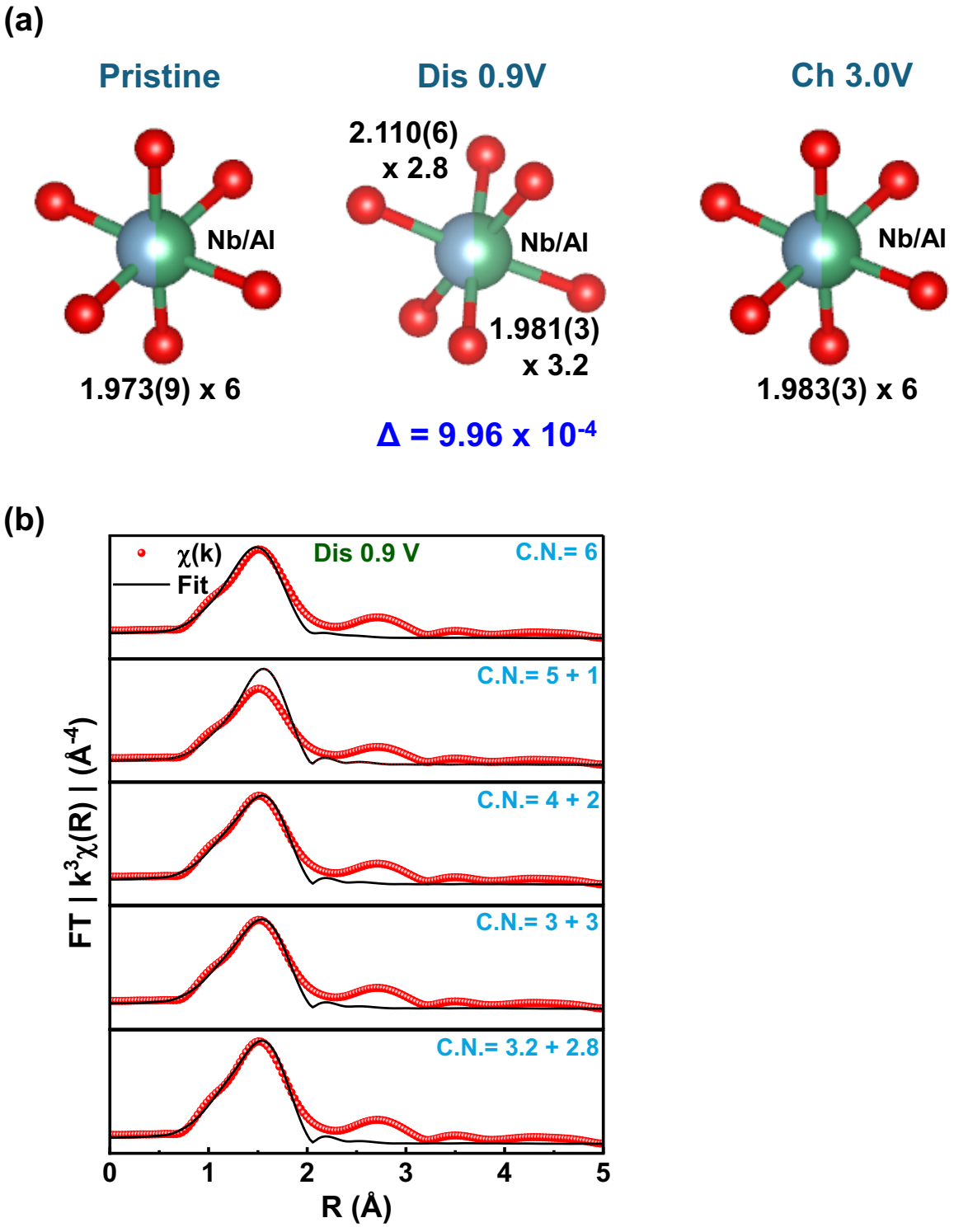

Figure S13. (a) Local coordination environment of Nb/AlO_6 octahedra in the pristine, discharged (0.9 V), and charged (3.0 V) states of the NASICON-NaNbAl anode. (b) Fourier-transformed EXAFS (FT-EXAFS) spectra of the NaNbAl anode at the discharged state (0.9 V), fitted using different coordination environments.

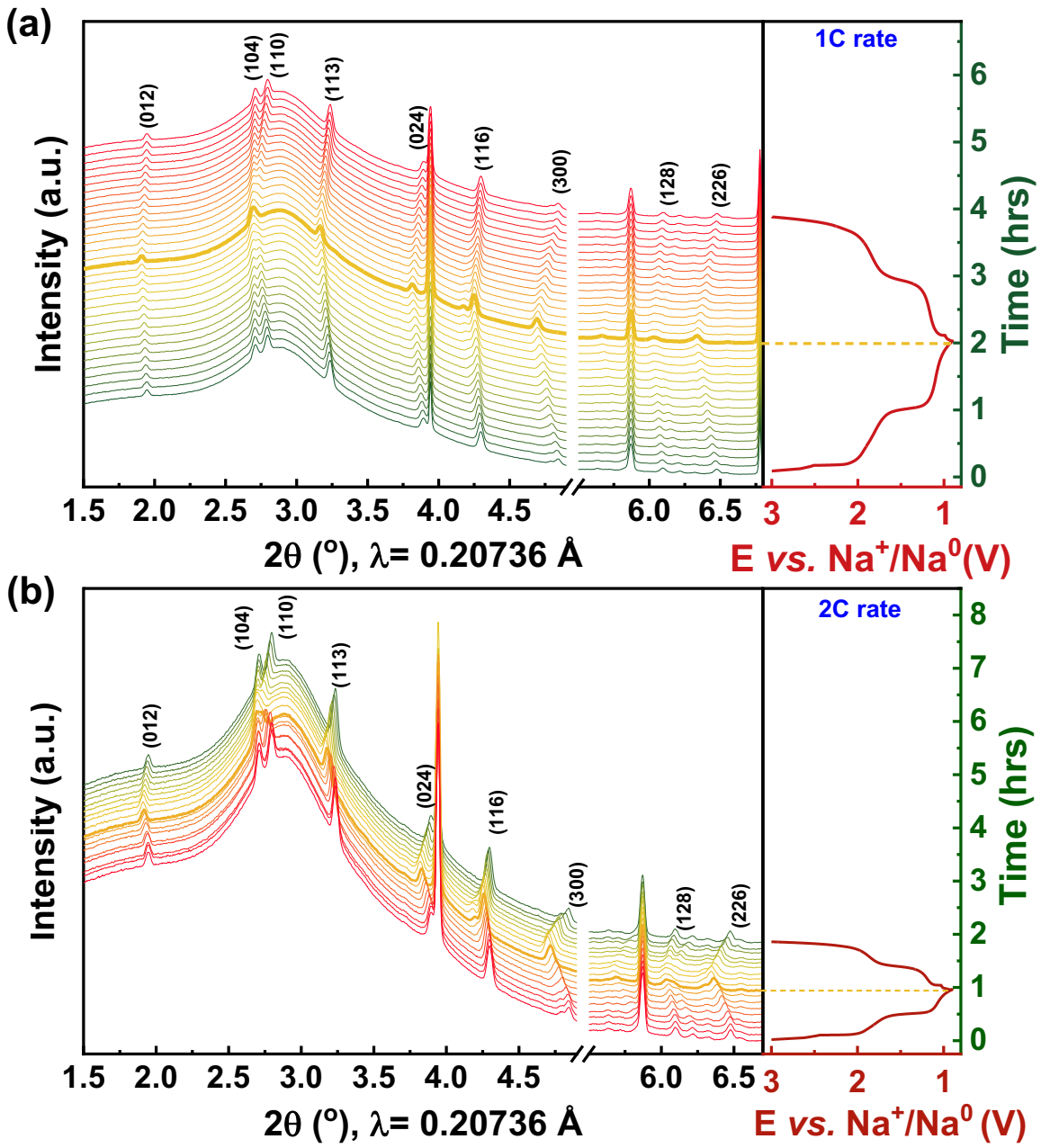

Figure S14. *Operando* XRD patterns of the NaNbAl anode collected at (a) 1C and (b) 2C rates at synchrotron facilities.

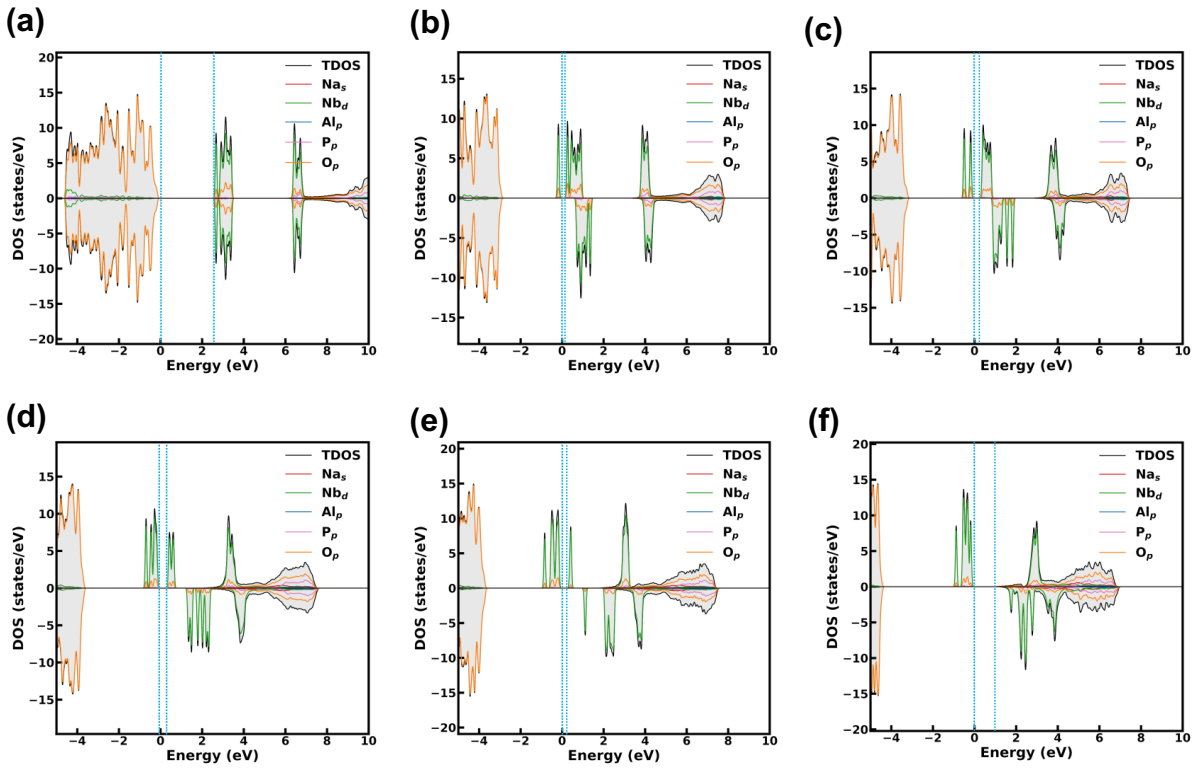

Figure S15. Projected and total density of states (PDOS and TDOS) for ground-state $Na_xNbAl(PO_4)_3$ compositions at (a) x = 1 (E_g = 2.48 eV), (b) x = 1.5 (E_g = 0.08 eV), (c) x = 2 (E_g = 0.21 eV), (d) x = 3 (E_g = 0.23 eV), (e) x = 3.5 (E_g = 0.21 eV), and (f) x = 4 (E_g = 0.87 eV), where E_g is the band gap. The zero of the energy scale is set at the valence band maximum, with the dotted cyan lines indicating the band edges. Positive and negative DOS states correspond to spin-up and spin-down states, respectively. The PDOS for Na *s*, Nb *d*, Al *p*, P *p*, and O *p* bands are represented by red, green, blue, pink, and orange colored curves.

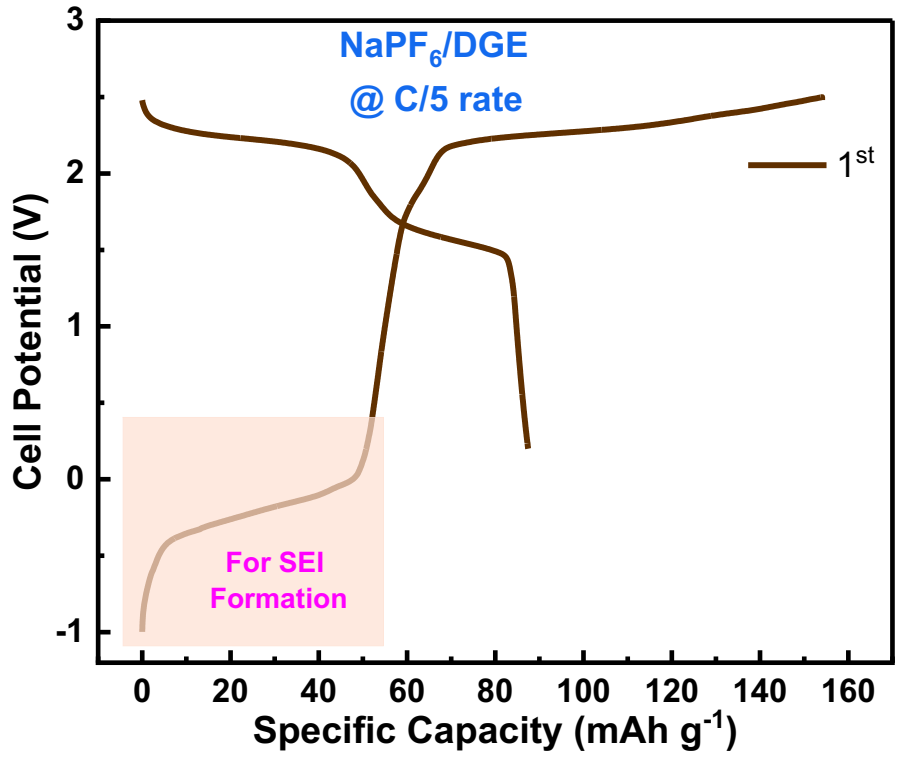

Figure S16. Voltage-capacity curve of the Na_4VP||NaNbAl full cell at C/5 rate during the first cycle.

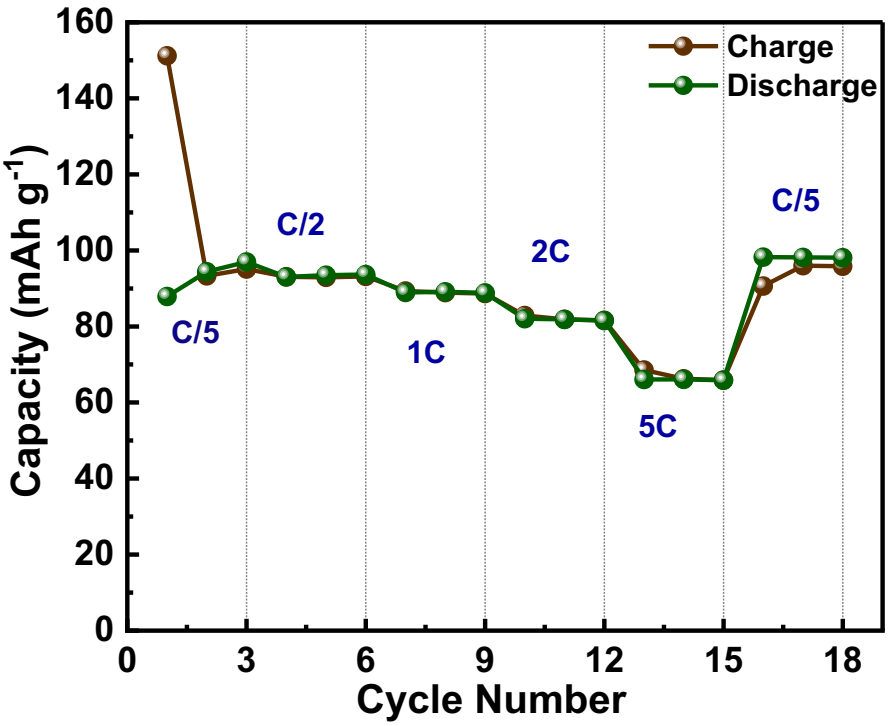

Figure S17. Rate Performances at various C rates C/5, C/2, 1C, 2C, and 5C of the Na_4VP||NaNbAl full cell.

Table S1. Crystallographic parameters obtained from the Rietveld refinement of XRD pattern of NaNbAl anode.

$NaNbAl(PO_4)_3$						
R_{wp} = 8.50%; R_p = 8.54%; R_{Bragg} = 4.68%						
Phase 1(95%): **NASICON-$NaNbAl(PO_4)_3$**; Space group: $R\bar{3}c$ (#167); Z = 6 a = 8.4801(9) Å; c = 21.7864(28) Å; c/a = 2.565. V = 1356.812(27) Å^3 ; V/Z = 226.136 Å^3						
Atom	**Wyck*off***	***x***	***y***	***z***	**Uiso, Å^2**	**Occupancy**
Nb	*12c*	*0.00000*	*0.00000*	*0.14288(3)*	0.012	0.5
Al	*12c*	*0.00000*	*0.00000*	*0.14288(3)*	0.012	0.5
P(1)	*18e*	*0.28220(18)*	*0.00000*	*0.25000*	0.045	1
Na(1)	*6b*	*0.00000*	*0.00000*	*0.00000*	0.095	0.858
Na(2)	*18e*	*0.72855(26)*	*0.00000*	*0.25000*	0.804	0.04
O(1)	*36f*	*0.19134(20)*	*0.16343(22)*	*0.09106(8)*	0.029	1
O(2)	*36f*	*0.02935(27)*	*0.19398(22)*	*0.19001(9)*	0.041	1
Phase 2 (5%): **$AlPO_4$**; Space group: $C222_1$ (#20) a = 7.12259 Å; b= 7.118465 Å; c = 6.969464Å V = 353.365 Å^3						
Atom	**Wyck*off***	***x***	***y***	***z***	**Uiso, Å^2**	**Occupancy**
Al	*4b*	*0.00000*	*0.27443*	*0.25000*	0.002	1.0
P	*4a*	*0.35691*	*0.00000*	*0.00000*	0.008	1.0
O(1)	*8c*	*0.16085*	*0.01758*	*0.14753*	0.001(3)	1.0
O(2)	*8c*	*0.19424*	*0.31553*	*0.97204*	0.006(2)	1.0

Table S2. Refined parameters for the first shell of Nb K-edge EXAFS spectra collected on the pristine, discharged and charge $NaNbAl(PO_4)_3$ anodes.

Sample	**Coordination Number**	**d(Nb-O) Å**	**E_0 (eV)**	**σ^2 Å^2**	**R-factor**
Pristine	6	1.973(9)	8.0	0.0058	0.002
Discharge 0.9V	3.2+2.8	2.110(6) x 2.8 1.981(3) x 3.2	8.0	0.0058	0.011
Charge 3.0 V	6	1.983(3)	6.9	0.0081	0.006

Table S3. Comparison of the electrochemical performance in this work with that of the reported Nb and V-based NASICON anodes for SIBs.

Anode	Particle Size	Average Voltage	Capacity (mAh g^{-1})	Rate Performance	Capacity Retention	Ref
$NaNbAl(PO_4)_3$	1-2 μm	1.44 V	125	125 mAh g^{-1} at C/10 120 mAh g^{-1} at C/5 113 mAh g^{-1} at C/2 106 mAh g^{-1} at 1C 98 mAh g^{-1} at 2C 85 mAh g^{-1} at 5C 65 mAh g^{-1} at 10C	92% @ 1C after 200 cycles 86% @ 5C after 1000 cycles	This work
$NaAlNb(PO_4)_3$/C	60-100 nm	1.52 V	117	117 mAh g^{-1} at C/10 95 mAh g^{-1} at C/5	86% @ C/10 after 30 cycles	[27]
$Na_{1.0}V_{0.25}Al_{0.25}Nb_{1.5}(PO_4)_3$/C	100-300 nm	1.4 V	140	139 mAh g^{-1} at C/5 135 mAh g^{-1} at C/2 130 mAh g^{-1} at 1C 127 mAh g^{-1} at 2C 120 mAh g^{-1} at 5C 109 mAh g^{-1} at 10C	98.3% @ 1C after 500 cycles 95.2% @ 10C after 5000 cycles	[25]
$Na_{1.5}V_{0.5}Nb_{1.5}(PO_4)_3$	0.8-3.4 μm	1.4 V	140	140 mAh g^{-1} at C/10 132 mAh g^{-1} at C/5	82% @ 1C after 200 cycles	[28]

				125 mAh g^{-1} at C/2 120 mAh g^{-1} at 1C 110 mAh g^{-1} at 2C 105 mAh g^{-1} at 5C	89% @ 5C after 500 cycles	
$NaNbV(PO_4)_3/C$	100-300 nm	1.55 V	180	174 mAh g^{-1} @ C/2 165 mAh g^{-1} @1C 160 mAh g^{-1} at 4C 144 mAh g^{-1} at 10C	93.9% @ 1C after 100 cycles 93.2% @ 10C after 150 cycles	[29]
$NaCrNb(PO_4)_3/C$	200-500 nm	1.52 V	170	170 mAh g^{-1} at C/10 158 mAh g^{-1} at C/5 153 mAh g^{-1} at C/2 148 mAh g^{-1} at 1C 142 mAh g^{-1} at 2C 125 mAh g^{-1} at 5C	82.6% @ 1C after 300 cycles	[30]
$Nb_2(PO_4)_3$	10 μm	1.46 V	150	172 mAh g^{-1} at C/10 163 mAh g^{-1} at C/5 153 mAh g^{-1} at C/2 144 mAh g^{-1} at 1C 129 mAh g^{-1} at 2C	60.2% @ 1C after 200 cycles	[31]
$Na_3V_2(PO_4)_3/C$	500-900 nm	1.63 V	50	50 mAh g^{-1} at C/5 42 mAh g^{-1} at 10C		[32]

References

[1] H. M. Rietveld, *J. Appl. Crystallogr.* **1969**, *2*, 65-71.

[2] J. Rodríguez-Carvajal, *Phys. B Condens. Matter* **1993**, *192*, 55-69.

[3] A. C. Dippel, H. P. Liermann, J. T. Delitz, P. Walter, H. Schulte-Schrepping, O. H. Seeck, H. Franz, *J. Synchrotron Radiat.* **2015**, *22*, 675-687.

[4] A. Schökel, M. Etter, A. Berghäuser, A. Horst, D. Lindackers, T. A. Whittle, S. Schmid, M. Acosta, M. Knapp, H. Ehrenberg, M. Hinterstein, *J. Synchrotron Radiat.* **2021**, *28*, 146-157.

[5] M. Herklotz, J. Weiß, E. Ahrens, M. Yavuz, L. Mereacre, N. Kiziltas-Yavuz, C. Dräger, H. Ehrenberg, J. Eckert, F. Fauth, L. Giebeler, M. Knapp, *J. Appl. Crystallogr.* **2016**, *49*, 340-345.

[6] O. Arcelus, J. Rodríguez-Carvajal, N. A. Katcho, M. Reynaud, A. P. Black, D. Chatzogiannakis, C. Frontera, J. Serrano-Sevillano, M. Ismail, J. Carrasco, F. Fauth, M. R. Palacin, M. Casas-Cabanas, *J. Appl. Crystallogr.* **2024**, *57*, 1676-1690.

[7] M. Newville, *J. Synchrotron. Radiat.* **2001**, *8*, 322-324.

[8] B. Ravel, M. Newville, *J. Synchrotron. Radiat.* **2005**, *12*, 537-541.

[9] G. Kresse, J. Furthmüller, *Phys. Rev. B* **1996**, *54*, 11169-11186.

[10] G. Kresse, J. Hafner, *Phys. Rev. B* **1993**, *47*, 558-561.

[11] J. Sun, A. Ruzsinszky, J. P. Perdew, *Phys. Rev. Lett.* **2015**, *115*, 036402.

[12] G. Kresse, D. Joubert, *Phys. Rev. B Condens. MatterMater. Phys.* **1999**, *59*, 1758-1775.

[13] S. P. Ong, W. D. Richards, A. Jain, G. Hautier, M. Kocher, S. Cholia, D. Gunter, V. L. Chevrier, K. A. Persson, G. Ceder, *Comput. Mater. Sci.* **2013**, *68*, 314-319.

[14] I. Batatia, P. Benner, Y. Chiang, A. M. Elena, D. P. Kovács, J. Riebesell, X. R. Advincula, M. Asta, M. Avaylon, W. J. Baldwin, *et al*., *arXiv preprint* **2024**, *arXiv:2401.00096*.

[15] I. Batatia, S. Batzner, D. P. Kovács, A. Musaelian, G. N. C. Simm, R. Drautz, C. Ortner, B. Kozinsky, G. Csányi, *Nat. Mach. Intell.* **2025**, *7*, 56-67.

[16] B. Singh, Z. Wang, S. Park, G. S. Gautam, J.-N. Chotard, L. Croguennec, D. Carlier, A. K. Cheetham, C. Masquelier, P. Canepa, *J. Mater. Chem. A* **2021**, *9*, 281-292.

[17] Z. Wang, S. Park, Z. Deng, D. Carlier, J.-N. Chotard, L. Croguennec, G. S. Gautam, A. K. Cheetham, C. Masquelier, P. Canepa, *J. Mater. Chem. A* **2022**, *10*, 209-217.

[18] G. Henkelman, B. P. Uberuaga, H. Jónsson, *J. Chem. Phys.* **2000**, *113*, 9901-9904.

[19] J. P. Perdew, K. Burke, M. Ernzerhof, *Phys. Rev. Lett.* **1996**, *77*, 3865-3868.

[20] R. Devi, B. Singh, P. Canepa, G. S. Gautam, *npj Comput. Mater.* **2022**, *8*, 160.

[21] J. Nocedal, *Math. Comput.* **1980**, *35*, 773-782.

[22] M. Neumann, J. Gin, B. Rhodes, S. Bennett, Z. Li, H. Choubisa, A. Hussey, J. Godwin, *arXiv preprint* **2024**, *arXiv:2410.22570*.

[23] B. Rhodes, S. Vandenhaute, V. Šimkus, J. Gin, J. Godwin, T. Duignan, M. Neumann, *arXiv preprint* **2024**, *arXiv:2504.06231*.

[24] A. K. Bheemaguli, P. Xiao, G. S. Gautam, *arXiv preprint* **2025**, *arXiv:2512.03642*.

[25] B. Patra, S. Narayanan, S. Halder, M. Sharma, D. Sachdeva, N. Ravishankar, S. K. Pati, S. K. Jain, P. Senguttuvan, *Adv. Mater.* **2025**, *5*, 2419417.

[26] W. Weppner, R. A. Huggins, *J. Electrochem. Soc.* **1977**, *124*, 1569-1578.

[27] I. R. Cherkashchenko, R. V. Panin, A. V. Babkin, D. A. Novichkov, E. V. Antipov, N. R. Khasanova, *Mendeleev Commun.* **2025**, *35*, 393-395.

[28] B. Patra, R. Hegde, A. Natarajan, D. Deb, D. Sachdeva, N. Ravishankar, K. Kumar, G. S. Gautam, P. Senguttuvan, *Adv. Energy Mater.* **2024**, *14*, 2304091.

[29] N. R. Khasanova, R. V. Panin, I. R. Cherkashchenko, M. V. Zakharkin, D. A. Novichkov, E. V. Antipov, *ACS Appl. Mater. Interfaces* **2023**, *15*, 30272.

[30] R. V. Panin, I. R. Cherkashchenko, V. V. Zaitseva, R. R. Samigullin, M. V. Zakharkin, D. A. Novichkov, A. V. Babkin, I. V. Mikheev, N. R. Khasanova, E. V. Antipov, *Chem. Mater.* **2024**, *36*, 6902-6911.

[31] B. Patra, K. Kumar, D. Deb, S. Ghosh, G. S. Gautam, P. Senguttuvan, *J. Mater. Chem. A* **2023**, *11*, 8173-8183.

[32] K. Saravanan, C. W. Mason, A. Rudola, K. H. Wong, P. Balaya, *Adv. Energy Mater.* **2013**, *3*, 444.